

## Measurements of the boron-to-carbon and boron-to-oxygen flux ratios in cosmic rays with DAMPE

**Chuan Yue,<sup>a,b,\*</sup> Zhan-Fang Chen,<sup>a,b</sup> Dimitrios Kyratzis,<sup>c,d,†</sup> Andrea Parenti,<sup>c,d</sup> Yi-Feng Wei<sup>e</sup> and Qiang Yuan<sup>a,b</sup> for the DAMPE collaboration**

<sup>a</sup>Key Laboratory of Dark Matter and Space Astronomy, Purple Mountain Observatory, Chinese Academy of Sciences, Nanjing 210034, China

<sup>b</sup>School of Astronomy and Space Science, University of Science and Technology of China, Hefei 230026, China

<sup>c</sup>Gran Sasso Science Institute (GSSI), Via Iacobucci 2, I-67100 L'Aquila, Italy

<sup>d</sup>Istituto Nazionale di Fisica Nucleare (INFN) - Laboratori Nazionali del Gran Sasso, I-67100 Assergi, L'Aquila, Italy

<sup>e</sup>State Key Laboratory of Particle Detection and Electronics, University of Science and Technology of China, Hefei 230026, China

E-mail: [yuechuan@pmo.ac.cn](mailto:yuechuan@pmo.ac.cn), [chenzf@pmo.ac.cn](mailto:chenzf@pmo.ac.cn), [dimitrios.kyratzis@gssi.it](mailto:dimitrios.kyratzis@gssi.it), [andrea.parenti@gssi.it](mailto:andrea.parenti@gssi.it), [weiyf@ustc.edu.cn](mailto:weiyf@ustc.edu.cn), [yuanq@pmo.ac.cn](mailto:yuanq@pmo.ac.cn)

Boron nuclei in cosmic rays (CRs) are believed to be mainly produced by the fragmentation of heavier nuclei, such as carbon and oxygen, via collisions with the interstellar matter. Therefore, the boron-to-carbon flux ratio (B/C) and the boron-to-oxygen flux ratio (B/O) are very essential probes of the CR propagation. With a large geometric factor and a good charge resolution, the Dark Matter Particle Explorer (DAMPE), is expected to extend the measurement of B/C and B/O up to a few TeV/n energies. In this contribution, the direct measurements of B/C and B/O in the energy range from 10 GeV/n to 5.6 TeV/n with six years of data collected by DAMPE are presented.

38th International Cosmic Ray Conference (ICRC2023)  
26 July - 3 August, 2023  
Nagoya, Japan



<sup>†</sup>Now at Department of Nuclear and Particle Physics, University of Geneva, CH-1211 Geneva, Switzerland

\*Speaker

## 1. Introduction

Cosmic rays (CRs) are typically divided into two classes: primary and secondary. Primary CRs are accelerated at astrophysical sources such as supernova remnants, while secondaries are produced from the interactions of the primaries with the interstellar medium (ISM) during the propagation. Precise measurements of the secondary-to-primary flux ratios are thus crucial to reliably constrain the propagation process of CRs [1, 2]. Among all the secondary-to-primary ratios, the B/C ratio is the most extensively measured. Thanks to the contributions from worldwide experiments, the B/C ratio has been measured up to a few TeV/n [3–13], although the uncertainties are relatively large for kinetic energies above 500 GeV/n. A power-law decline form,  $\propto \mathcal{R}^{-1/3}$ , can well fit the rigidity (energy) dependence of the B/C ratio [9], in agreement with the prediction of the Kolmogorov turbulence [14]. Improved measurements of the secondary-to-primary ratios, especially towards higher energies, are highly necessary to further understand the propagation of CRs and the properties of the interstellar medium.

The DARK Matter Particle Explorer (DAMPE; also known as “Wukong”) is a calorimetric-type, satellite-borne detector for high energy cosmic-ray and  $\gamma$ -ray observations [15]. The DAMPE detector consists of 4 sub-detectors [15], which are a Plastic Scintillator strip Detector (PSD), a Silicon-Tungsten trackER-converter(STK), a BGO imaging calorimeter and a Neutron Detector (NUD) from top to bottom, as shown in Fig. 1. With its relatively large geometric factor, good charge [16] and energy resolution [15], DAMPE is expected to extend the precise measurements of individual spectra of high-abundance CR species from protons to Iron nuclei up to a few hundreds of TeV energies [17, 18]. In this study, the direct measurements of B/C and B/O in the energy range from 10 GeV/n to 5.6 TeV/n with six years of data collected by the DAMPE is presented. More details on the analysis and a deeper discussion of the results can be found in [19].

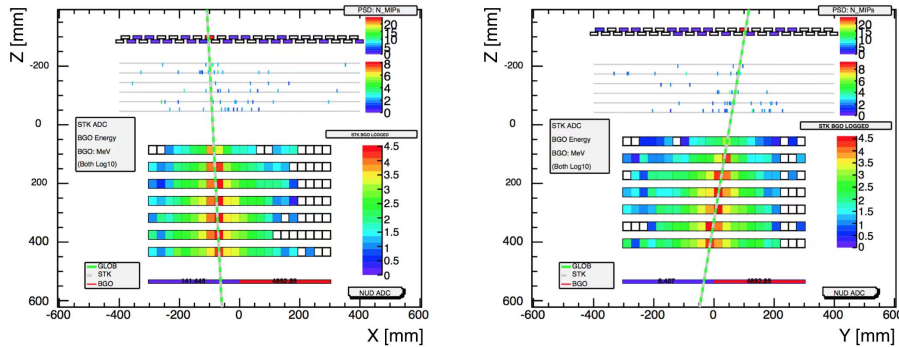


**Figure 1:** A schematic side view of the DAMPE payload. An example of an on-orbit boron candidate is superimposed to illustrate the shower development in the subdetectors.

## 2. Data analysis

Six years of DAMPE on-orbit data from January 1<sup>st</sup>, 2016 to December 31<sup>st</sup>, 2021 are analyzed in this work. The live time fraction is about 75.9% after excluding the instrument dead time, the time for the on-orbit calibration, the time in the South Atlantic Anomaly (SAA) region, and the

period between September 9, 2017 and September 13, 2017 during which a big solar flare affected the status of the detector [20].

## 2.1 MC Simulations

Extensive MC simulations are carried out to estimate the instrument response of incident particles in the DAMPE detector. In this work, the GEANT toolkit v4.10.05 [21] with the FTFP\_BERT physics list is adopted for the simulations of nuclei. For higher energies we link the EPOS\_LHC model by means of a CRMC-GEANT4 interface [22]. The energy response of MC simulations is tuned by including the Birks' quenching [23, 24] for the ionization energy deposits in the BGO calorimeter, due to secondary particles with a large charge number and a low kinetic energy. The simulated events are generated assuming an isotropic source with an  $E^{-1.0}$  spectrum. In the analysis, the simulation data are re-weighted to  $E^{-2.6}$  and  $E^{-3.0}$  spectra, for primary (e.g. carbon and oxygen) and secondary (e.g. boron) nuclei, respectively. For boron nuclei,  $^{10}\text{B}$  and  $^{11}\text{B}$  samples are mixed assuming an isotopic composition of  $Y_{\text{B}} = ^{11}\text{B}/(^{11}\text{B} + ^{10}\text{B}) = 0.7$ , according to the AMS-02 low energy measurements [9]. As an evaluation of the uncertainties from the hadronic interaction model, we also perform simulations with the FLUKA 2011.2x package [25], which uses DPMJET3 for nucleus-nucleus interaction above 5 GeV/n. The same analysis procedure based on the two simulations are carried out, and the final differences of the B/C and B/O ratios are taken as systematic uncertainties from the hadronic interaction model.

## 2.2 Event Selection

DAMPE implements four different triggers on orbit [26], among which the high-energy (HE) trigger is chosen to select events for the CR spectral analysis. The events with total deposited energy in the BGO calorimeter ( $E_{\text{BGO}}$ ) higher than 80 GeV are selected to avoid the geomagnetic rigidity cut-off effect. To ensure a good shower containment, the BGO crystal with the maximum energy deposition in each of the first six layer is required not to be at the edge of the calorimeter.

The trajectory of an incident particle is obtained by optimizing the multiple STK tracks reconstructed with the Kalman filter algorithm [27]. The quality of the track is evaluated by jointly considering the number of hits on the track, the  $\chi^2/\text{dof}$  value of the Kalman filter, the signal consistency of each hit, and the deviation between the track and the shower axis in the calorimeter. In case that several good track candidates are found, the one with the maximum average hit energy is chosen. The selected track is then required to pass the PSD with maximum energy in both  $X$  and  $Y$  views, and pass through the calorimeter from top to bottom.

The particle charge  $Z$  is reconstructed with the ionization energy deposited in both PSD and STK. We first require the charge value from the hit of the first STK plane along the track to be larger than 4 ( $Q_{\text{STK1st}} > 4$ ), in order to effectively suppress particles lighter than boron. Then we employ the PSD hits on the selected track to calculate the particle charge. A detailed charge reconstruction algorithm is applied for each hit based on its ionization energy deposition, including the path length correction, the light attenuation correction and the light yield saturation correction [16, 28]. We eliminate the energy-dependence of the charge measurements, primarily due to back-scattered secondaries whose signals add up to the primary particle's ionization signal, via setting the peaks to corresponding integer charge values. The PSD charge hits on the trajectory are further selected by

a consistency requirement of  $|\Delta Z| < 1$  (sub-layer by sub-layer from top to bottom). The final PSD charge value is obtained by averaging the charge measurements from the selected PSD hits, which achieves a good energy-independence as shown in Fig. 2(a). The same procedure is applied to the MC simulations, and the MC charge distributions are shrunk to match the flight data. Fig. 2(b) illustrates the MC template fit of the charge distribution for deposited energies in the calorimeter of 1TeV to 1.58 TeV. The boron, carbon and oxygen candidates are selected with energy-independent charge intervals of [4.7, 5.3], [5.6, 6.5] and [7.6, 8.5], respectively. After the charge selection, we have  $1.16 \times 10^5$  boron,  $1.27 \times 10^6$  carbon and  $2.17 \times 10^6$  oxygen candidates with  $E_{\text{BGO}} > 80$  GeV.

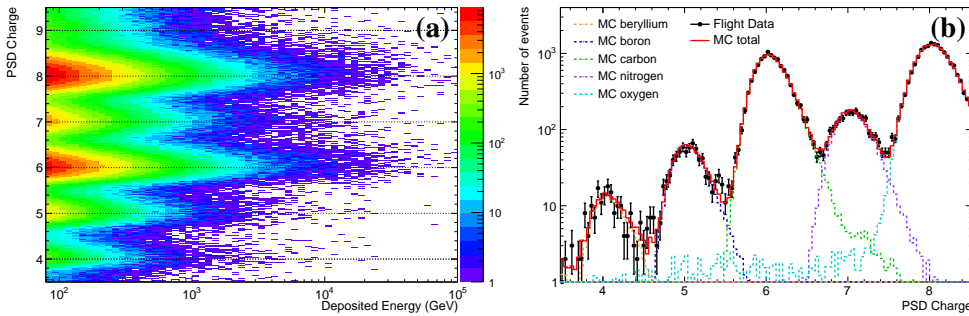


**Figure 2:** The PSD charge as a function of the deposited energy for particles with  $Z = 4 - 8$  in flight data (a) and the MC template fit of the charge distribution for deposited energies in the calorimeter of 1TeV to 1.58 TeV (b).

### 2.3 Background

The background is dominated by the mis-identification of particle charge, primarily due to the fragmentation in PSD. We employ the MC charge distributions as templates to fit the flight data (see Fig. 2(b)) and estimate the background contributions. The background from nuclei heavier than fluorine is neglected in this analysis, as their fluxes are much lower than those of carbon and oxygen. The contamination of the boron sample is found to be 1% to 2% for  $E_{\text{BGO}} < 1$  TeV and  $\sim 4.5\%$  around 50 TeV, while the contamination of the carbon and oxygen sample is less than 1.0% and 1.6% respectively, over the entire energy range.

### 2.4 Energy measurement and spectral unfolding

The deposited energy  $E_{\text{BGO}}$  is obtained as the sum of the energy deposit in each crystal of the calorimeter. The rare BGO readout saturation for very high energy events, typically above 20 TeV, is corrected via the method in [29]. The BGO energy response to nuclei was studied at CERN SPS in 2014-2015 using beams of accelerated ion fragments with  $A/Z = 2$  and kinetic energies of 40 and 75 GeV/n[30]. The energy response matrices for carbon and oxygen are shown in Fig. 3, together with the distributions of the deposited energy fraction for test beams with  $E_k = 75$  GeV/n. The comparisons between the beam test data and the GEANT4 FTFP\_BERT simulations shows a good agreement within the statistical uncertainties. Due to the energy leakage of hadronic shower in the calorimeter because of its limited thickness, the energy resolution for nuclei measurements is

not as good as for electrons/photons. Furthermore, the deposited energy fraction shows a decrease trend with the increase of the incident energy. An unfolding procedure is thus necessary to account for the bin-to-bin migration effect. The observed number of events,  $N_{\text{obs},i}$ , in the  $i$ -th deposited energy bin is related to the incident number of events,  $N_{\text{inc},j}$ , in the  $j$ -th incident energy bin via the response matrix  $M$  as

$$N_{\text{obs},i}(1 - \beta_i) = \sum_j M_{ij} N_{\text{inc},j}, \quad (1)$$

where  $\beta_i$  is the background fraction,  $M_{ij}$  is the probability that particles in the  $j$ -th incident energy bin contributing to the  $i$ -th deposited energy bin. The response matrix is derived using MC simulations after applying the same selection procedure as for the flight data. In this work, we use the Bayesian unfolding approach [31] to derive the incident numbers of events. The uncertainty of the energy response matrix, mainly due to the uncertainty of the hadronic interaction model, is estimated through a comparison between different MC simulations, i.e. GEANT4 and FLUKA, and is included in the systematic uncertainties.

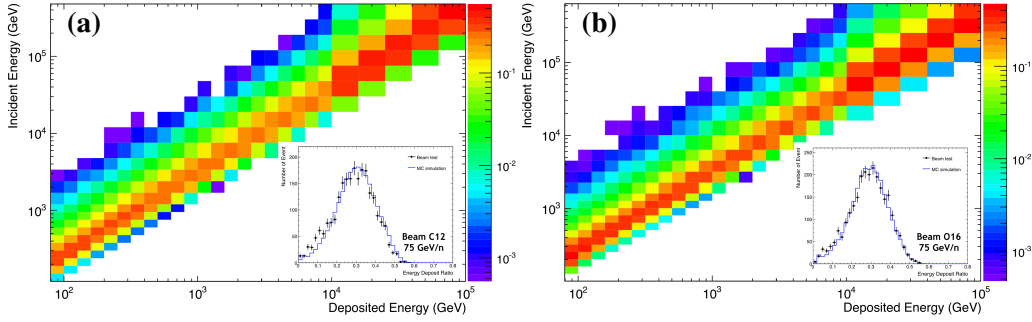


**Figure 3:** The energy response matrices for carbon (a) and oxygen (b). The comparisons of the deposited energy fraction between the test beam data at CERN-SPS and the GEANT4 FTFP\_BERT simulations with  $E_k = 75$  GeV/n are overlotted.

## 2.5 Flux ratio calculation

In order to obtain the flux ratio as a function of the kinetic energy per nucleon ( $E_k$ ), the atomic mass numbers are averaged by assuming an isotope composition from AMS measurements [9] for boron, pure  $^{12}\text{C}$  for carbon and pure  $^{16}\text{O}$  for oxygen. The flux ratio of B/C (B/O) in the  $i$ -th  $E_k$  bin is given by

$$R_i = \frac{\Phi_i^{\text{B}}}{\Phi_i^{\text{C(O)}}} = \frac{N_i^{\text{B}}}{N_i^{\text{C(O)}}} \left( \frac{\varepsilon_i^{\text{B}}}{\varepsilon_i^{\text{C(O)}}} \right)^{-1}, \quad (2)$$

where  $N_i^{\text{B}}$  and  $N_i^{\text{C(O)}}$  are the unfolded numbers of boron and carbon (oxygen) nuclei,  $\varepsilon_i^{\text{B}}$  and  $\varepsilon_i^{\text{C(O)}}$  are the total selection efficiencies derived from MC simulations. The efficiencies are also validated with the flight data, with deviations being treated as systematic uncertainties.

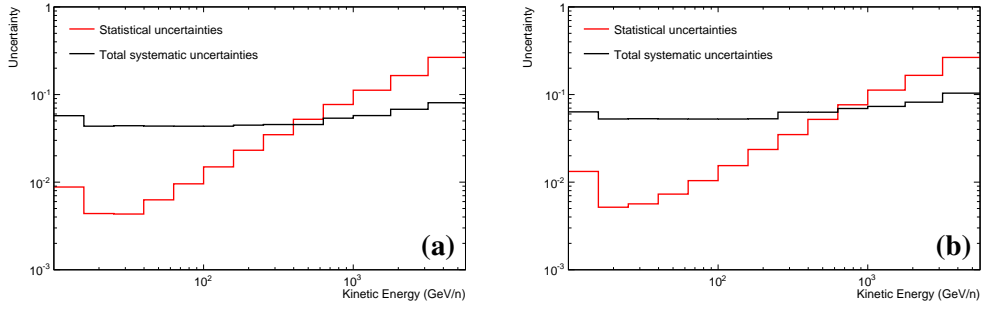


**Figure 4:** Relative uncertainties of B/C (a) and B/O (b) as a function of the kinetic energy per nucleon.

## 2.6 Uncertainty analysis

The statistical uncertainties refer to the Poisson fluctuations of the measured number of events in each deposited energy bin. To obtain a proper estimate of the full error propagation in the unfolding procedure, we employ a toy-MC approach by sampling the deposited energy spectrum with Poisson fluctuations, and get the variations of the unfolded numbers of events in each incident energy bin. The root-mean-squares of the resulting B/C and B/O variations are taken as the  $1\sigma$  statistical uncertainties. The systematic uncertainties are investigated extensively in this analysis. Main sources of systematic uncertainties for the flux ratio measurements include the trigger efficiency, the charge selection, the background subtraction, the isotope composition of boron, the unfolding procedure, and the hadronic model. The total systematic uncertainties are computed as the quadratic sum of all the components, as shown in Fig. 4. The systematic uncertainties dominate over the statistical ones for energies below  $\sim 1$  TeV/n and vice versa for high energies.

## 3. Results

The B/C and B/O ratios in the energy range from 10 GeV/n to 5.6 TeV/n are shown in Fig. 5. The atomic mass numbers are assumed to be 10.7 (see Ref. [9]), 12, and 16 for boron, carbon, and oxygen, respectively. Compared with previous measurements, the DAMPE measurements are well consistent with them at low energies ( $E_k \lesssim 500$  GeV/n) and improve the precision significantly at high energies. Particularly, the DAMPE results provide the precise measurements of the B/C and B/O ratios above 1 TeV/n.

The energy dependence of both the B/C and B/O ratios can be well fitted by a broken power-law model rather than a single power-law model, suggesting the existence in both flux ratios of a spectral hardening at about 100 GeV/n. The best fits of the BPL model based on the nuisance parameter method [19] are illustrated in Fig. 5. The fitting parameters and a comprehensive discussion can be found in [19]. The significance of the break is about  $5.6\sigma$  and  $6.9\sigma$  for the GEANT4 simulation, and  $4.4\sigma$  and  $6.9\sigma$  for the alternative FLUKA simulation, for B/C and B/O, respectively. The detection of spectral hardenings in the B/C and B/O ratios by DAMPE deviate from the predictions of conventional turbulence theories of the interstellar medium. The measurements can imply a change of turbulence properties of the interstellar medium (ISM) at different scales or novel propagation

effects of CRs [32], and should be properly incorporated in the indirect detection of dark matter via anti-matter particles [33].

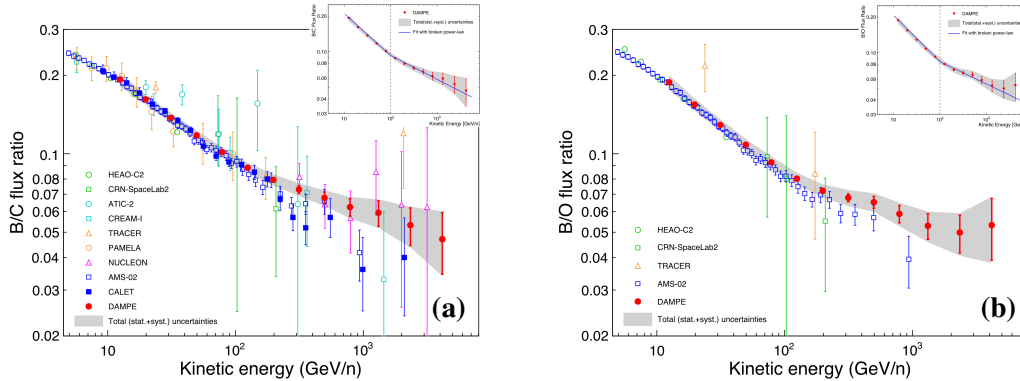


**Figure 5:** Boron-to-carbon (a) and boron-to-oxygen (b) flux ratios as functions of kinetic energy per nucleon [19]. DAMPE measurements are shown by red filled dots, with error bars and shaded bands representing the statistical and total uncertainties, respectively. The total uncertainties are the sum in quadrature of the statistical and systematic ones. In panel (a), other direct measurements by HEAO3 [3], CRN [4], ATIC-2 [5], CREAM-I [6], TRACER [7], PAMELA [8], NUCLEON-KLEM [10], AMS-02 [12] and CALET [13] are shown for comparison. In panel (b), the measurements of B/O by HEAO3 [3], CRN [4], TRACER [7] and AMS-02 [12] are shown.

#### 4. Acknowledgements

The DAMPE mission is funded by the Strategic Priority Science and Technology Projects of CAS. In China, the data analysis was supported by the National Key Research and Development Program of China (No. 2022YFF0503302) and the National Natural Science Foundation of China (Nos. 12220101003, 11921003, 11903084, 12003076 and 12022503), the CAS Project for Young Scientists in Basic Research (No. YSBR061), the Youth Innovation Promotion Association of CAS, the Young Elite Scientists Sponsorship Program by CAST (No. YESS20220197), and the Program for Innovative Talents and Entrepreneur in Jiangsu. In Europe the activities and data analysis are supported by the Swiss National Science Foundation (SNSF), Switzerland, the National Institute for Nuclear Physics (INFN), Italy, and the European Research Council (ERC) under the European Union’s Horizon 2020 research and innovation programme (No. 851103).

#### References

- [1] A. W. Strong, I. V. Moskalenko, V. S. Ptuskin, *Annu. Rev. Nucl. Part. S* **57**, 285-327 (2007).
- [2] J. Becker Tjus, L. Merten, *Phys. Rept.* **872**, 1-98 (2020).
- [3] J. J. Engelmann, P. Ferrando, A. Soutoul, *et al.*, *Astron. Astrophys.* **233**, 96-111 (1990).
- [4] S. P. Swordy, D. Mueller, P. Meyer, *et al.*, *Astrophys. J.* **349**, 625 (1990).

- [5] A. D. Panov, N. V. Sokolskaya, J. H. Adams, *et al.*, International Cosmic Ray Conference **2**, 3 (2008).
- [6] H. S. Ahn, P. S. Allison, M. G. Bagliesie, *et al.*, Astropart. Phys. **30**, 133-141 (2008).
- [7] A. Obermeier, M. Ave, P. Boyle, *et al.*, Astrophys. J. **742**, 14 (2011).
- [8] O. Adriani, G. C. Barbarino, G. A. Bazilevskaya, *et al.*, Astrophys. J. **791**, 93 (2014).
- [9] M. Aguilar, *et al.* (AMS Collaboration), Phys. Rev. Lett. **117**, 231102 (2016).
- [10] V. Grebenyuk, D. Karmanov, I. Kovalev I, *et al.*, Adv. Space. Res. **64**, 2559-2563 (2019).
- [11] M. Aguilar, *et al.* (AMS Collaboration), Phys. Rev. Lett. **120**, 021101 (2018).
- [12] M. Aguilar, *et al.* (AMS Collaboration), Phys. Rept. **894**, 1-116 (2021).
- [13] O. Adriani, *et al.* (CALET Collaboration), Phys. Rev. Lett. **129**, 251103 (2022).
- [14] A. Kolmogorov, Akademiia Nauk SSSR Doklady **30**, 301-305 (1941).
- [15] J. Chang, G. Ambrosi, Q. An, *et al.*, Astropart. Phys. **95**, 6-24 (2017).
- [16] T.-K. Dong, Y.-P. Zhang, P.-X. Ma, *et al.*, Astropart. Phys. **105**, 31-36 (2019).
- [17] Q. An, *et al.* (DAMPE Collaboration), Sci. Adv. **5**, eaax3793 (2019).
- [18] F. Alemanno, *et al.* (DAMPE Collaboration), Phys. Rev. Lett. **126**, 201102 (2021).
- [19] DAMPE Collaboration, Sci. Bull. **67**, 2162-2166 (2022)
- [20] F. Alemanno, *et al.* (DAMPE Collaboration), Astrophys. J. Lett. **920**, L43 (2021).
- [21] C. Agostinelli, *et al.* (GEANT4 Collaboration), Nucl. Instrum. Meth. A. **506**, 250-303 (2003).
- [22] A. Tykhonov *et al.*, Proceedings of ICRC2019 **PoS(ICRC2019)**, 143 (2019).
- [23] J. B. Birks, Proceedings of the Physical Society. Section A **64**, 874–877 (1951).
- [24] Y. Wei *et al.*, IEEE Trans. Nucl. Sci. **67**, 939–945 (2020).
- [25] T. T. Böhlen, F. Cerutti, M. P. W Chin, *et al.*, Nucl. Data Sheets **120**, 211-214 (2014).
- [26] Y.-Q. Zhang *et al.*, Res. Astron. Astrophys. **19**, 123 (2019).
- [27] A. Tykhonov *et al.*, Nucl. Instrum. Meth. A. **893**, 43–56 (2018).
- [28] P.-X. Ma *et al.*, Res. Astron. Astrophys. **19**, 082 (2019).
- [29] C. Yue *et al.*, Nucl. Instrum. Meth. A. **984**, 164645 (2020).
- [30] Y. Wei *et al.*, Nucl. Instrum. Meth. A. **922**, 177–184 (2019).
- [31] G. D’Agostini, Nucl. Instrum. Meth. A. **362**, 487–498 (1995).
- [32] P.-X. Ma, Z.-H. Xu, Q. Yuan, *et al.*, Front. Phys. **18**, 44301 (2023)
- [33] M.-Y. Cui, Q. Yuan, S.-Y.-L. Tsai, *et al.*, Phys. Rev. Lett. **118**, 191101 (2016).